Journal of Advanced Research (2015) 6, 555–562

Cairo University

Journal of Advanced Research

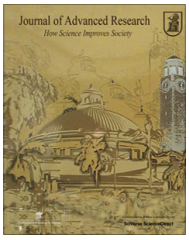

ORIGINAL ARTICLE

Electrical and optical properties of nickel ferrite/polyaniline nanocomposite

M. Khairy [a], **M.E. Gouda** [b,*]

[a] *Chemistry Department, Faculty of Science, Benha University, Benha, Egypt*
[b] *Physics Department, Faculty of Science, Benha University, Benha, Egypt*

ARTICLE INFO

Article history:
Received 2 October 2013
Received in revised form 19 January 2014
Accepted 21 January 2014
Available online 27 January 2014

Keywords:
Nanoparticle
Composite materials
Polyaniline
Electrical conductivity
Optical properties

ABSTRACT

Polyaniline–$NiFe_2O_4$ nanocomposites (PANI–$NiFe_2O_4$) with different contents of $NiFe_2O_4$ (2.5, 5 and 50 wt%) were prepared via in situ chemical oxidation polymerization, while the nanoparticles nickel ferrite were synthesized by sol–gel method. The prepared samples were characterized using some techniques such as Fourier transforms infrared (FTIR), X-ray diffraction (XRD), scanning electron microscopy (SEM) and thermogravimetric analysis (TGA). Moreover, the electrical conductivity and optical properties of the nanocomposites were investigated. Pure (PANI) and the composites containing 2.5 and 5 wt% $NiFe_2O_4$ showed amorphous structures, while the one with 50 wt% $NiFe_2O_4$ showed a spinel crystalline structure. The SEM images of the composites showed different aggregations for the different nickel ferrite contents. FTIR spectra revealed to the formation of some interactions between the PANI macromolecule and the $NiFe_2O_4$ nanoparticles, while the thermal analyses indicated an increase in the composites stability for samples with higher $NiFe_2O_4$ nanoparticles contents. The electrical conductivity of PANI–$NiFe_2O_4$ nanocomposite was found to increase with the rise in $NiFe_2O_4$ nanoparticle content, probably due to the polaron/bipolaron formation. The optical absorption experiments illustrate direct transition with an energy band gap of $E_g = 1.0$ for PANI–$NiFe_2O_4$ nanocomposite.

Introduction

The study of nanocomposite materials is a rapidly developing subject of research. This fast growing area is generating many inspiring new high-performance materials with new properties. Nanocomposite materials extensively cover a large range of systems such as one-dimensional, two-dimensional, three-dimensional and amorphous materials, made of definitely different components and mixed at the nanometer size. Large attempt is focused on the capability to attain rule of the nanoscale structures via new preparation methods. The properties of nanocomposite materials based not only on the properties of their particular parents, but also on their morphology and interfacial types [1]. The applications of nanocomposites are quite promising in the fields of microelectronic packaging, optical integrated circuits, automobiles, drug delivery, sensors, injection molded products, membranes, packaging materials, aerospace, coatings, adhesives, fire-retardants, medical devices, consumer goods, etc. [2]. Polymer materials in the form of nanocomposites are useful due to certain advantages such as high surface area to volume ratio.

* Corresponding author. Tel.: +20 1028387722.
E-mail address: mostafagouda88@yahoo.com (M.E. Gouda).
Peer review under responsibility of Cairo University.

Production and hosting by Elsevier

2090-1232 © 2014 Production and hosting by Elsevier B.V. on behalf of Cairo University.
http://dx.doi.org/10.1016/j.jare.2014.01.009

There has been a growing interest in new ways of producing conducting polymer nanocomposites that can exhibit some novel properties. A number of groups have reported studies on the electrical conductivity of composites of a variety of conducting polymers [3]. They found that the conductivity depends on several factors such as the type of filler, its concentration, size, concentration and the strength of the interaction between the filler molecules and the polymer macromolecules [4,5].

The conducting polymers are a new group of synthetic polymers which combines the chemical and mechanical properties of polymers with the electronic properties of metals and semiconductors [6]. Nowadays, conducting polymers have several applications in different areas such as microwave absorption, electronic displays, corrosion protection coating, electrochemical batteries, super capacitors, sensors, and electrodes [7–11]. They have extended p-conjugation with single- and double-bond alteration along its chain. They behave as a semiconductor material with low charge carrier mobility [12] and their conductivity is increased to reach the metallic range by doping with appropriate dopants [12]. Polyaniline is the most widely studied conducting polymer because of its facile synthesis, low synthetic cost, good environmental and thermal stability. There are three forms of PANI, namely, the fully reduced (leucoemeraldine), the fully oxidized (pernigraniline) state and the more conducting emeraldine base (half-oxidized). Emeraldine is the most conductive form when doped to form emeraldine salt [12].

Polyaniline can be easily prepared either chemically or electrochemically from acidic aqueous solutions [13,14]. The chemical method has a large significance because it is very reasonable method for the mass production of PANI. The most common preparation method is by oxidative polymerization with ammonium peroxodisulfate as an oxidant.

Ferrites belong to a special class of magnetic materials, which have a wide range of technological applications. Due to their low cost, ferrite materials are used in various devices like microwave, transformer cores, magnetic memories, isolators, noise filters, etc. [15–18]. The spin-glass state in ferrites exhibits the most interesting magnetic property that causes high field irreversibility, shift of the hysteresis loops, and anomalous relaxation dynamics [19,20].

Nickel ferrite ($NiFe_2O_4$) is one of the most important spinel ferrites that have been studied. Stoichiometric $NiFe_2O_4$ considers as n-type semicoductor [21]. It exhibits different kinds of magnetic properties such as paramagnetic, superparamagnetic or ferrimagnetic behavior depending on the particle size and shape. Also, it exhibits unusual physical and chemical properties when its size is reduced to nano size.

Recently, significant scientific and technological interest has focused on the PANI–inorganic nanocomposites. The use of nano sized inorganic fillers into the PANI matrix produces materials with complementary behavior between PANI and inorganic nanoparticles. These novel materials find applications in many industrial fields. The nanocomposites of polyaniline can be synthesized by polymerization of aniline in the presence of dispersed inorganic material. This can be done by three different routes [22]. The first route consists of direct solid-state mixing between the inorganic particles and the polyaniline macromolecules. The second one is in situ chemical polymerization of aniline in an acidic medium with dispersion of inorganic material in the presence of an oxidant at low temperature. The third route includes the dipping of the partially oxidized PANI in a suspension of the metal oxide.

The present study reports the synthesis, characterizations and effects of nano sized $NiFe_2O_4$ addition on structural, thermal stability, optical and electrical properties of polyaniline.

Experimental

Materials

Aniline (Adwic 99%) was used after double distillation. Other chemicals used were of AR grade. Water used in this investigation was de-ionized water.

The nickel ferrite nanopowder was synthesized by sol–gel method. An appropriate amounts of nickel nitrate ($Ni(NO_3)_2{\cdot}6H_2O$) and ferric nitrate ($Fe(NO_3)_3{\cdot}9H_2O$) were mixed together with citric acid and polyethylene glycol (PEG) with 1:2:4.44:8.88 molar ratio of $Ni(NO_3)_2{\cdot}6H_2O$, $Fe(NO_3)_3{\cdot}9H_2O$, citric acid and PEG, respectively. The solution obtained was vigorously stirred during heating from room temperature to 90 °C, and kept for two hours. The solution became viscous and gel is formed. The gel was then washed with de-ionized water several times to remove possible residues and then dried at 110 °C for 24 h and calcined at 400 °C for 2 h.

$NiFe_2O_4$–PANI composite was prepared by the oxidation of aniline with ammonium peroxydisulphate in an aqueous medium. Aniline (0.2 M) was dissolved in 100 mL of HNO_3 (1 M) and stirred well in an ice bath. Certain amounts of $NiFe_2O_4$ nanopowder were suspended in the above solution and stirred for about one hour. As an oxidizing agent, 20 ml of pre-cooled solution of ammonium persulfate (0.25 M) was then slowly added drop wise to the mixture with a constant stirring over a period of 2 h. The reaction was then left at 0 °C for 4 h. The product obtained was collected by filtration and washed several times by acetone and distilled water until the filtrate was colorless. The product was dried at 80 °C for 24 h. Three different PANI–$NiFe_2O_4$ composites were prepared by using 2.5, 5 and 50 wt% $NiFe_2O_4$ with respect to the aniline monomer. Pure polyaniline was synthesized in the same manner without adding $NiFe_2O_4$.

Characterization

XRD spectra of pure PANI, $NiFe_2O_4$ and PANI–$NiFe_2O_4$ composites were performed at room temperature in the range from 2θ = 10–80° on a Diano (made by Diano Corporation, USA), using Cu Kα radiation (λ = 1.5406 Å). The infrared spectra of the specimens were recorded using a KBr pellet on a Brucker-FTIR (Vector 22), made in Germany. SEM of the pure PANI and PANI–$NiFe_2O_4$ composite was recorded using JEOL JSM 6400 microscope. TGA thermograms of pure PANI, $NiFe_2O_4$ and PANI–$NiFe_2O_4$ composites were recorded under nitrogen atmosphere and in a temperature range of 25–600 °C and at a heating rate of 10 °C/min using Shimadzu DT-50 thermal analyzer. Conductivity measurements were performed on pellets of 1.3 cm and 0.15 cm thickness in the temperature range of 30–250 °C. The optical absorption of composites dissolved in dimethyl sulfoxide (DMSO) was measured at room temperature on UV/vis spectrophotometer (T80 + PG) in the range of 400–1100 nm.

Results and discussion

X-ray diffraction

XRD of $NiFe_2O_4$, PANI–$NiFe_2O_4$ composite and PANI are given in Fig. 1. $NiFe_2O_4$ showed the main diffraction patterns characterized for cubic spinel (JCPDS Card No. 10-0325) [23]. The spectra did not show any other peaks for impurities. The broadening nature of the diffraction peaks refers to the small dimensions of the particles prepared. The crystallite size was estimated using Debye–Scherrer formula: $D = 0.9\lambda/\beta\cos\theta$ where D is the mean crystallite size, λ is the wavelength of Cu Kα, β is the full width at half maximum (FWHM) of the diffraction peaks and θ is the Bragg's angle. The average crystallite size is found to be about 20 nm. The X-ray diffraction pattern of PANI, Fig. 1b, shows amorphous nature in partially crystalline state with two diffraction peaks of at about $2\theta = 20.3°$ and 25.1°. The planes of Benzinoid and Quinoid rings of PANI chain are responsible for crystalline structure [24]. However, XRD pattern of PANI-2.5 wt% $NiFe_2O_4$ composite shows diffraction peaks almost similar to the free PANI (Fig. 1c). This refers to the distortion of $NiFe_2O_4$ crystal structure during the polymerization reaction causing the transformation of the crystalline $NiFe_2O_4$ into an amorphous state; and hence the XRD peaks of PANI are predominating [25]. On the other hand, the XRD patterns of the composite with a high concentration of $NiFe_2O_4$ (50 wt% $NiFe_2O_4$), Fig. 1d shows a crystalline phase with an average particle size of 17 nm comparable with that found for the sample containing 2.5 wt% $NiFe_2O_4$ (13 nm).

The effect of $NiFe_2O_4$ addition on the degree of crystallinity in the composites has been tested using the peak intensity of XRD of $NiFe_2O_4$ in the composite samples. The degree of crystallinity was found to increase with increasing the amount of $NiFe_2O_4$ (Fig. 1).

FTIR spectra

The FTIR spectra of the nano-sized $NiFe_2O_4$, PANI and PANI-50 wt% $NiFe_2O_4$ composite (dried at 60 °C) are shown in Fig. 2a and b. For $NiFe_2O_4$ sample two main broad metal–oxygen (Fe—O) stretching vibrations are observed at 588 and 412 cm^{-1}, which correspond to intrinsic stretching vibrations of the metal–oxygen at the tetrahedral- and octahedral-site, respectively. These absorption bands represent characteristic features of spinel ferrites in single phase [26].

The FT-IR spectra of PANI showed band at around 3235 cm^{-1} attributed to the protonation of amines functional group at polymer backbone (N—H stretching), bands at 1577 and 1490 cm^{-1} attributed to C=C stretching deformation of quinonoid and benzenoid units of PANI, respectively. The peak appearing at 1294 cm^{-1} corresponds to C—N stretching of secondary amine in polymer main chain, and the band observed at 1125 cm^{-1} is attributed to in plane bending vibration of C—H mode. All the observed peaks were similar to those of pure polyaniline prepared by a common method [27]. However, the FT-IR spectra of the composite samples showed that the peaks of both PANI (1301 and 1139 cm^{-1}) and $NiFe_2O_4$ (655 and 527 cm^{-1}) are shifted to higher wave number.

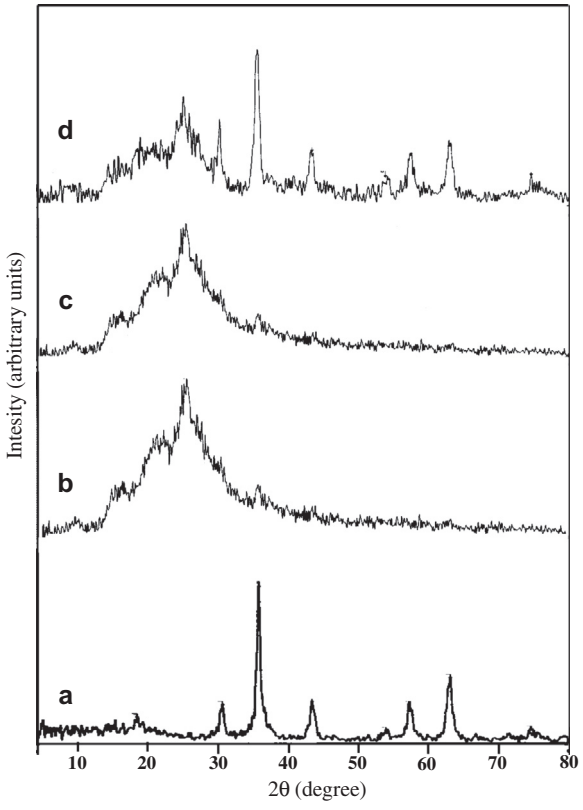

Fig. 1 XRD pattern of: a – $NiFe_2O_4$, b – PANI, c – PANI-2.5% $NiFe_2O_4$, d – PANI-50% $NiFe_2O_4$.

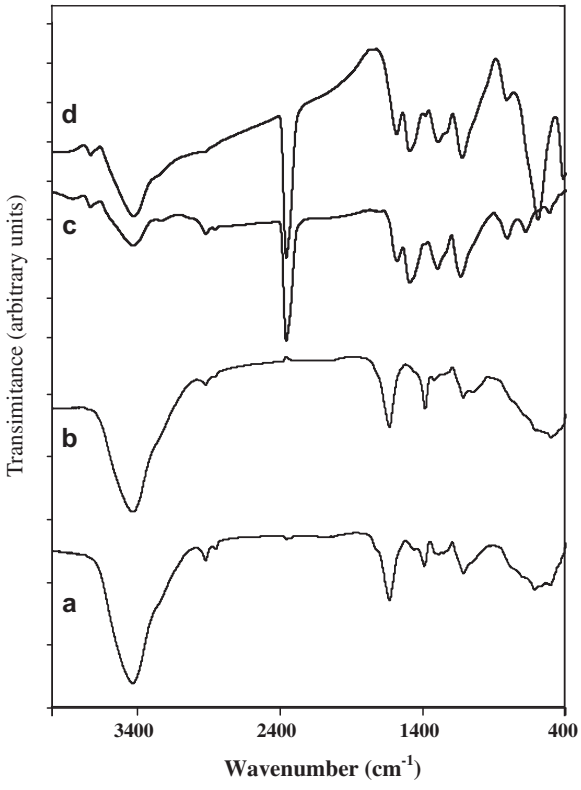

Fig. 2 FTIR spectra of: a – PANI at 60 °C, b – PANI-50% $NiFe_2O_4$ at 60 °C, c – PANI at 170 °C, d – PANI-50% $NiFe_2O_4$ at 170 °C.

Moreover, two new bands related to stretching vibration of M—N were observed at 655 and 527 cm^{-1}. The above results reveal to the presence of some interactions between PANI chains and nickel ferrite particles.

The FTIR spectrum for composite samples dried at 170 °C is also shown in Fig. 2c and d. It shows greater difference than that of virgin samples. This refers to some dissociation occurring in the investigated samples as will be shown in thermal analyses results.

Morphology of the composites

Fig. 3 shows the surface morphologies of the PANI, $NiFe_2O_4$ and the PANI–$NiFe_2O_4$ composites. SEM-image of PANI shows homogeneous particle shapes appearing as insects of fibers. SEM-image of nano $NiFe_2O_4$ particles shows spherical shapes with high homogeneity, while SEM image of the PANI-50 wt% $NiFe_2O_4$ composite shows a completely different image where the surface appearing as tree leaf shape. This may be attributed to that the nanoparticles of $NiFe_2O_4$ act as nuclei during the polymerization of aniline causing a formation of a homogeneous cluster of PANI. The nanosized particles of $NiFe_2O_4$ would be distributed in each of the surface and the bulk of the composite [28,29].

Thermal stability

Fig. 4 shows the TGA curves of PANI and PANI–$NiFe_2O_4$ nanocomposites. All curves show a three step weight loss. For all samples, the first step just below 70 °C is accompanied by a weight loss of about 15%. This is probably due to the moisture evaporation, which are trapped inside the polymer or bound to the surface of polymer backbone (physisorbed water molecules) [30]. The removing of water is easier in the composite with higher surface area or with increasing the interfaces between their particles [31]. The second weight loss lie between 115 and 275 °C with a weight loss ranges from 13% to 17%. This may be attributed to the release of dopant anions compensated the positive charge of PANI chains. The last decomposition stage starts at temperature higher than 275 °C with a weight loss ranges between 56% and 77%. This is due to the complete decomposition of the organic part of the composites.

The decomposition temperatures (T_d) showed an increase in T_d for PANI (380 °C) with increasing the amount of $NiFe_2O_4$ to reach a value of 430 °C for sample containing 50 wt% nickel ferrite. This indicates that the introducing of $NiFe_2O_4$ into PANI matrix increases its thermal stability which agrees well with the results obtained by Wang et al. [32].

DC-conductivity

The temperature dependence of dc-conductivity (σ_{dc}) for $NiFe_2O_4$, PANI and PANI/$NiFe_2O_4$ composites in a temperature range between 30 and 250 °C is illustrated in Fig. 5. It is clear from the Fig. 5 that, the conductivity values of investigated composites are higher than that found for each of pure $NiFe_2O_4$ and pure PANI. The σ_{dc} increases steadily with temperature showing semiconductor behavior up to a transition temperature T_t. The observed T_t was found to be 155 °C for PANI and 150, 160 and 120 °C for the composites containing

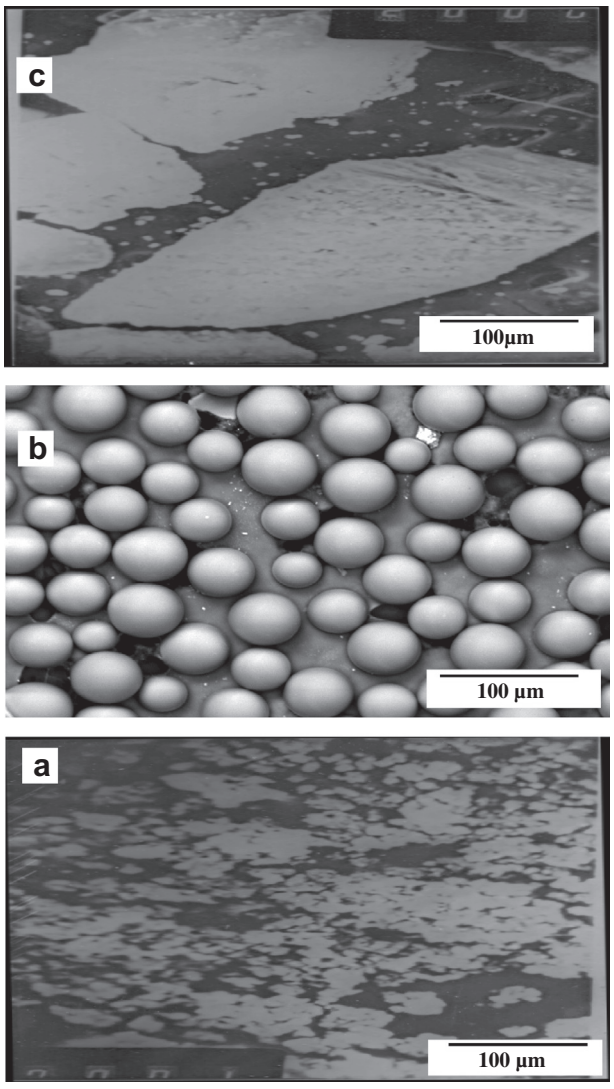

Fig. 3 SEM of: a – PANI, b – $NiFe_2O_4$, c – PANI-50% $NiFe_2O_4$.

2.5, 5 and 50 wt% $NiFe_2O_4$, respectively, Fig. 5. The figure shows also that at temperature higher than T_t, σ_{dc} decreases gradually. A similar trend has been reported for similar systems [33,34]. The decrease in conductivity after the well noticeable transition temperature (T_t) is attributed to the release of the dopant ions from the polymer structure, as confirmed by thermal analyses.

More looking, in Fig. 5 shows that the conductivity increases with increasing $NiFe_2O_4$ content to attain an almost constant value at higher concentrations of ferrite.

To explain the conductive behavior in our samples we suggested the formation of polarons upon oxidation of polyaniline molecule and the combination of two close polarons to form bipolaron [35,36]. The net effect is the formation of a doubly charged defect (bipolaron) delocalized over several rings of polyaniline. On increasing $NiFe_2O_4$ content, the conductivity changes slightly in the range of 0.55–0.76 S cm^{-1} (Table 1), which attributed to saturation of charge carriers. However, for higher $NiFe_2O_4$ contents, the conductivity is mostly affected by two factors: (1) The insulating behavior

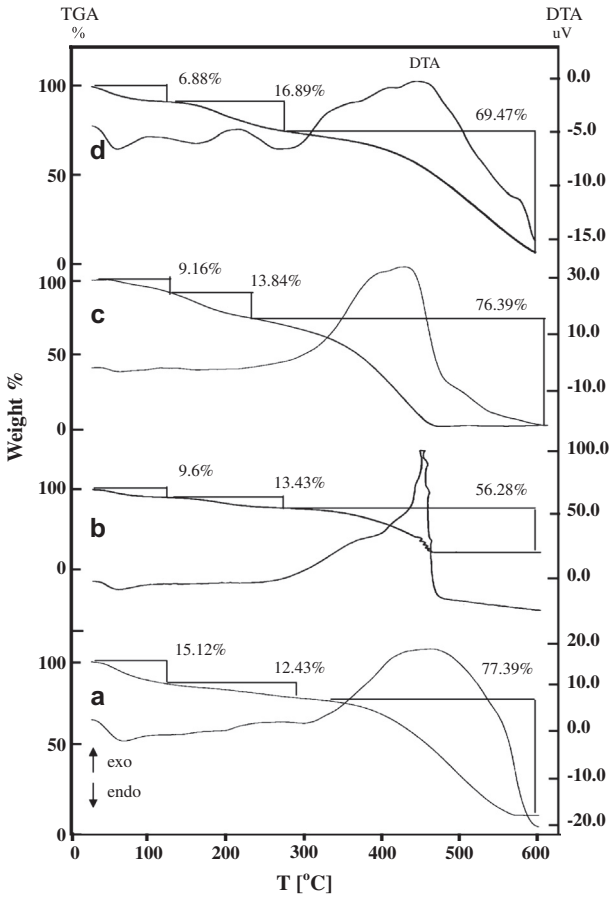

Fig. 4 TGA and DTA of: a – PANI, b – PANI-2.5% $NiFe_2O_4$, c – PANI-5% $NiFe_2O_4$, d – PANI-50% $NiFe_2O_4$.

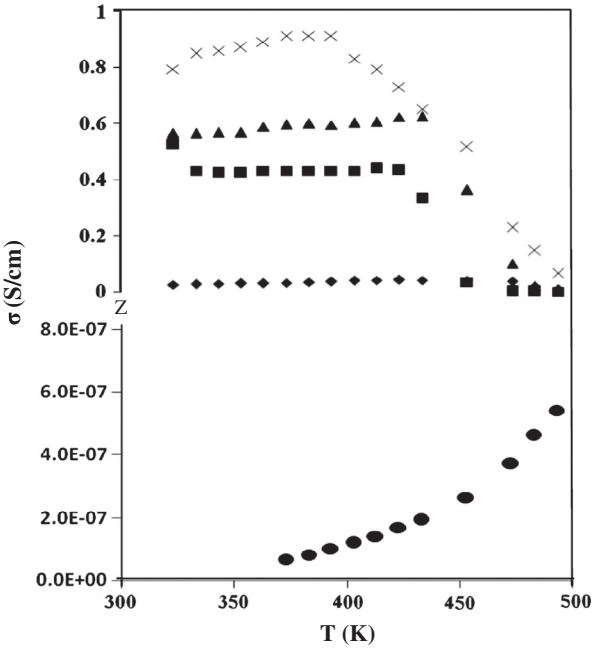

Fig. 5 Effect of temperature on the conductivity of: ♦, PANI; ■, PANI-2.5% $NiFe_2O_4$; ▲, PANI-5% $NiFe_2O_4$; x, PANI-50% $NiFe_2O_4$ and ●, Pure $NiFe_2O_4$.

of ferrite particles in the core of composites which hinders the charge transfer and blockage the conductivity path leads to lower conductivity of the polymer [37,38]. (2) The increase in $NiFe_2O_4$ content also increases the degree of crystallinity, and subsequently reduces the density of states at Fermi level which enhances the charge carrier mobility and gives rise to the conductivity [35,39].

To investigate the conduction mechanism, several models are applied for the conductivity data at temperatures below T_t. Greave's model showed the best fitting for the experimental data, Fig. 6. According to this model, the conductivity is attributed to the hopping of charge carriers in three-dimensional between localized states at the Fermi level. It can be expressed by [40,41]:

$$\sigma_{dc}(T) = \sigma_o T^{-1/2} exp(-T/T)^{1/4} \quad (1)$$

where σ_o is a constant independent on temperature and T_o is the Mott characteristics temperature and has the formula

$$T_o = 16/(kN(E_f)L^3) \quad (2)$$

where L is the localization length and $N(E_f)$ is the density of states and is estimated by assuming L value of 3 Å for aniline momomer [42]. The values obtained are given in Table 1. The estimated values of $N(f)$ for PANI–$NiFe_2O_4$ composites are decreases as the $NiFe_2O_4$ content increases. This is due to the increase in the crystallinity of the composites with increase in the concentration of nickel ferrite, as confirmed by X-ray diffraction.

The mean hopping distance R_{hopp} between two adjacent sites through a barrier height W_{hopp} is calculated by the following equations [41]

$$R_{hopp} = (3/8)L(T_o/T)^{1/4} \quad (3)$$

$$W_{hopp} = (1/4)kT(T_o/T)^{1/4} \quad (4)$$

Both R_{hopp} and W_{hop} for PANI–$NiFe_2O_4$ composites increase with increasing ferrite content, as shown in Table 1. This is interpreted according to increasing the charge carrier scattering at PANI–$NiFe_2O_4$ interfaces with increasing the amount of ferrite.

Optical absorption

The optical absorption spectrum is a significant method to attain optical energy band gap of crystalline and amorphous materials. The vital absorption, which corresponds to the electron excitation from the valance band to the conduction band, is used to verify the character and value of the optical band gap. At present, nano nickel ferrite as a filler semiconductor in PANI polymer has been used to make a red shift to the absorbed light.

UV–visible spectra of synthesized specimens were performed in the 400–1100 nm range, (Fig. 7). Positions of the observed optical absorption peaks have been calculated by the second derivative of absorbance–wavelength relationship, and the attained results are listed in Table 2.

The spectrum of PANI shows a single absorption peak at 578 nm, which is attributed to polaron/bipolaron transition. While the spectra of PANI–$NiFe_2O_4$ composites show tow peaks, the first one appeared in the range 558–590 nm is

Table 1 Electrical conductivity data.

Sample	σ_{dc} (at 300 K) S cm^{-1}	T_o (K)	R (Å)	W (eV)	$N(E)$ (eV^{-1} cm^{-3})
Pure PANI	2.27×10^{-2}	2.71×10^{6}	10.96	0.063	2.5×10^{21}
PANI-2.5 wt% $NiFe_2O_4$	5.51×10^{-1}	1.72×10^{4}	3.09	0.018	4.0×10^{23}
PANI-2.5 wt% $NiFe_2O_4$	6.31×10^{-1}	5.43×10^{4}	4.13	0.024	1.3×10^{23}
PANI-2.5 wt% $NiFe_2O_4$	7.63×10^{-1}	2.49×10^{5}	6.04	0.034	2.8×10^{22}

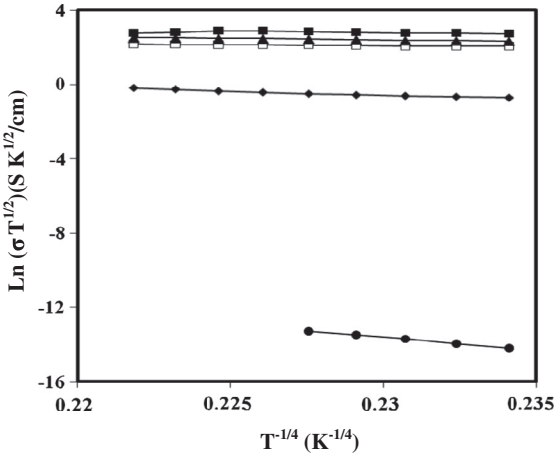

Fig. 6 Application of Graves's model on the conductivity data of: ♦, PANI; □, PANI-2.5% $NiFe_2O_4$; ▲, PANI-5% $NiFe_2O_4$; ■, PANI-50% $NiFe_2O_4$ and ●, Pure $NiFe_2O_4$.

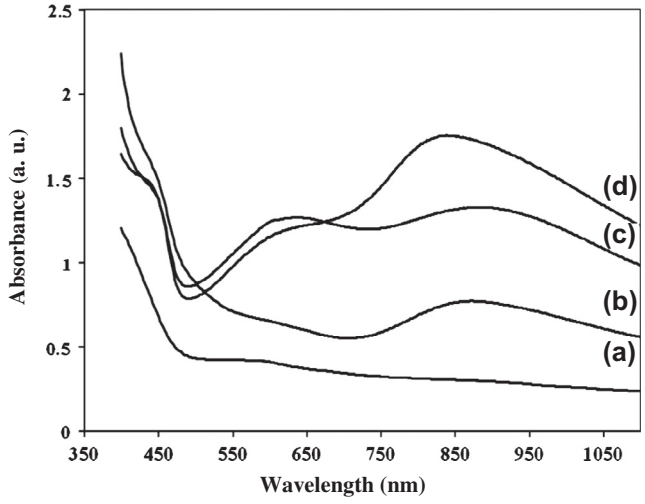

Fig. 7 UV–vis spectra of: (a) PANI, (b) PANI-5% $NiFe_2O_4$, (c)PANI-50% $NiFe_2O_4$, (d) PANI-2.5% $NiFe_2O_4$.

attributed to the exciton transition from the benzenoid to quinoid rings (π–π^*) transition and the second peak observed in the range 808–876 nm is due to polaron/bipolaron transition [35,43]. The absorption peaks of the composites are slightly shifted to longer wave length with increasing the ferrite content in the sample. This can be attributed to energy confinement produced from surface plasmon-excitation interaction as a result of the formation of ferrite–polymer core shell. These core shells increase the absorption cross section of the nano composite and thus enhance plasma-exciton interactions [44–46].

Table 2 Optical data determined for the studied samples.

Sample	Peak position (nm)		E_g (eV)
	P_1	P_2	
Pure PANI	–	578	2.7
PANI-2.5 wt% $NiFe_2O_4$	558	808	1
PANI-5 wt% $NiFe_2O_4$	558	838	1
PANI-50 wt% $NiFe_2O_4$	590	876	1

The optical band gap is determined using the following relationship [47]

$$(\alpha h\nu)^{1/n} = A(h\nu - E_g) \quad (5)$$

where α is the absorption coefficient, A is constant, E_g is the optical band gap of the material and the exponent n depends on the nature of electronic transition, it is equal to 1/2 for direct allowed, 3/2 for direct forbidden transitions and 2 for indirect allowed transition. The kind of transition is investigated by determining the power n that showed a value of $n = 1/2$ revealing to direct allowed transition. The E_g-value is calculated using the least square fitting of Eq. (5) and listed in Table 2. It is evident that the direct band gap E_g values for composites are unchanged and equal to 1.0 eV. The optical band gap E_g for pure PANI is found to be 2.7 eV, which agrees well with the published data [48,49].

Conclusions

PANI–$NiFe_2O_4$ nanocomposites were successfully prepared by in situ polymerization with excellent electrical, thermal and optical properties. The combined results of TGA, FTIR and UV–vis spectra showed that nickel ferrite nanoparticles enhanced the thermal stability of the composites, referring to the presence of some interaction between ferrite particles and PANI. FTIR and XRD results of composites confirmed that the addition of the nickel ferrite nanoparticles did not damage the backbone structure of PANI and the presence of nickel ferrite as a spinel in the amorphous structure of PANI. The conductivity of composites increased with increasing $NiFe_2O_4$ in the sample. It is attributed to the polaron/bipolaron formation. The conduction mechanism has been explained according to the three-dimensional hopping model proposed by Greaves. New optical absorption band due to plasmon–exciton interaction was observed in near IR of absorption spectra with $E_g = 1.0$ eV for the direct band transition. The results obtained refer to that specific properties can be tailored in the nanocomposites by mixing different proportions of PANI and $NiFe_2O_4$ nanoparticles.

Conflict of interest

The authors have declared no conflict of interest.

Compliance with Ethics Requirements

This article does not contain any studies with human or animal subjects.

References

[1] Kamigaito O. What can be improved by nanometer composites? J Jpn Soc Powder Metal 1991;38:315–21.

[2] Song F, Shen X, Liu M, Xiang J. Preparation and magnetic properties of $SrFe_{12}O_{19}/Ni_{0.5}Zn_{0.5}Fe_2O_4$ nanocomposite ferrite microfibers via sol–gel process. Mater Chem Phys 2011;126:791–6.

[3] Anilkumar RK, Parveen A, Badiger GR, Prasad MVNA. Effect of molybdenum trioxide (MoO_3) on the electrical conductivity of polyaniline. Physica B 2009;404:1664–7.

[4] Kryszewaski M. Heterogeneous conducting polymeric systems: dispersions, blends, crystalline conducting networks – an introductory presentation. Synth Metals 1991;45:289–96.

[5] Blaszkiewicz M, Mclachian DS, Newnham R. The volume fraction and temperature dependence of the resistivity in carbon black and graphite polymer composites: an effective media–percolation approach. J Polym Eng Sci 1992;32:421–5.

[6] Anand J, Palaniappan S, Sathyanarnayana DN. Conducting polyaniline blends and composites. Prog Polym Sci 1998;23:993–1018.

[7] Akel TM, Pienimaa S, Taka T, Jussila S, Isotalo H. Thin polyaniline films in EMI shielding. Synth Metals 1997;85:1335–6.

[8] Lu X, Ng HY, Xu J, Chaobin H. Electrical conductivity of polyaniline–dodecylbenzene sulphonic acid complex: thermal degradation and its mechanism. Synth Metals 2002;128:167–78.

[9] Kan JQ, Pan XH, Chen C. Polyaniline–uricase biosensor prepared with template process. Biosens Bioelectron 2004;19:1635–40.

[10] Ahmad N, MacDiarmid AG. Inhibition of corrosion of steels with the exploitation of conducting polymers. Synth Metals 1996;78:103–10.

[11] Rose TL, Antonio SD, Jillson MH, Kron AB, Suresh R, Wang F. A microwave shutter using conductive polymers. Synth Metals 1997;85:1439–40.

[12] Gupta K, Jana PC, Meikap AK. Electrical transport and optical properties of the composite of polyaniline nanorod with gold. Solid State Sci 2012;14:324–9.

[13] Gospodinova N, Terlemezyan L. Conducting polymers prepared by oxidative polymerization: polyaniline. Prog Polym Sci 1998;23:1443–84.

[14] Mathew RJ, Yang DL, Mattes BR. Effect of elevated temperature on the reactivity and structure of polyaniline. Macromolecules 2002;35:7575–81.

[15] Hashim M, Alimudin, Kumar S, Shirsath SE, Mohamed EM, Chunge H, et al. Studies on the activation energy from the ac conductivity measurements of rubber ferrite composites containing manganese zinc ferrite. Physica B 2012;407(21):4097–103.

[16] Goldman A. Modern ferrite technology. 2nd ed. New York: Springer; 2006.

[17] Shirsath SE, Kadam RH, Patange SM, Mane ML, Ghasemi A, Morisako A. Enhanced magnetic properties of Dy^{3+} substituted Ni–Cu–Zn ferrite nanoparticles. Appl Phys Lett 2012;100:042407–10.

[18] Narayanaswamy A, Sivakumar N. Influence of mechanical milling and thermal annealing on electrical and magnetic properties of nanostructured Ni–Zn and cobalt ferrites. Bull Mater Sci 2008;31:373–80.

[19] Raj K, Moskowitz B, Casciari R. Advances in ferrofluid technology. J Magn Magn Mater 1995;149:174–80.

[20] Kodama RH, Seaman CL, Berkowitz AE, Maple MB. Low-temperature magnetic relaxation of organic coated $NiFe_2O_4$ Particles. J Appl Phys 1994;75:5639–41.

[21] Baruwati B, Reddy K, Manorama S, Singh R, Parkash O. Tailored conductivity behavior in nanocrystalline nickel ferrite. Appl Phys Lett 2004;85:2833–5.

[22] Gemeay AH, Mansour IA, El-Sharkawy RG, Zaki AB. Preparation and characterization of polyaniline/manganese dioxide composites via oxidative polymerization: effect of acids. J Euro Poly 2005;41:2575–83.

[23] Costa ACFM, Leite AMD, Ferreira HS, Kiminami RHGA, Cavac S, Gama L. Brown pigment of the nanopowder spinel ferrite prepared by combustion reaction. J Euro Ceram Soc 2008;28:2033–7.

[24] Abdiryim T, Xiao-Gang Z, Jamal R. Comparative studies of solid-state synthesized polyaniline doped with inorganic acids. Mater Chem Phys 2005;90:367–72.

[25] Gemeay AH, El-Sharkawy RG, Mansour IA, Zaki AB. Preparation and characterization of polyaniline/manganese dioxide composites and their catalytic activity. J Colloid Interf Sci 2007;308:385–94.

[26] Waldron RD. Infrared spectra of ferrites. Phys Rev 1955;99:1727–35.

[27] Jiang J, Liangchao L, Feng X. Polyaniline–LiNi ferrite core–shell composite: preparation, characterization and properties. Mater Sci Eng A 2007;456:300–4.

[28] Biswas M, Ray SS, Liu Y. Water dispersible conducting nanocomposites of poly(*N*-vinylcarbazole), polypyrrole and polyaniline with nanodimensional manganese (IV) oxide. Synth Metals 1999;105:99–105.

[29] Ray SS, Biswas B. Water-dispersible conducting nanocomposites of polyaniline and poly(*N*-vinylcarbazole) with nanodimensional zirconium dioxide. Synth Metals 2000;108:231–6.

[30] Gok A, Sari B, Talu M. Synthesis and characterization of conducting substituted polyanilines. Synth Metals 2004;142:41–8.

[31] Peokes J, Trchova M, Hlavata D, Stejskal J. Conductivity ageing in temperature-cycled polyaniline. Poly Degrad Stab 2002;78:393–401.

[32] Wang S, Tan Z, Li Y, Sun L, Zhang T. Synthesis, characterization and thermal analysis of polyaniline/ZrO_2 composites. Thermochim Acta 2006;441:191–4.

[33] Mzenda VM, Goodman SA, Awet FD, Prinsloo LC. Characterization of electrical charge transfer in conducting polyaniline over the temperature range $300 < T(K) < 450$. Synth Metals 2002;127:279–83.

[34] Murugesan R, Subramanian E. The effect of Cu(II) coordination on the structure and electric properties of polyaniline–poly(vinyl alcohol) blend. Mater Chem Phys 2003;77:860–7.

[35] Sambhu B, Nikhil KS, Dipak K. Electrochemical synthesis of polyaniline and its comparison with chemically synthesized polyaniline. J Appl Poly Sci 2007;104:1900–4.

[36] Samrana K, Vazid A, Zulfequar M, Mazharul HM, Husain M. Electrical, thermal and spectroscopic studies of Te doped polyaniline. Curr Appl Phys 2007;7:68–75.

[37] Baykal A, Günay M, Toprak MS, Sozeri DH. Effect of ionic liquids on the electrical and magnetic performance of polyaniline–nickel ferrite nanocomposite. Mater Res Bull 2013;48:378–82.

[38] Aphesteguy JC, Bercoffb PG, Jacobo SE. Preparation of magnetic and conductive Ni–Gd ferrite–polyaniline composite. Phys B 2007;398:200–3.

[39] Qion Z, Jiew W, Yuliang M, Chuanbo C, Fang W. The relationship of conductivity to the morphology and crystallinity of polyaniline controlled by water content via reverse microemulsion. Colloid Polym Sci 2007;285:405–11.
[40] Ramaprasad AT, Vijayalakshmi R. Electronic conduction mechanism in chitin–polyaniline blend. Synth Metals 2008;158:1047–53.
[41] Mott N, Davis E. Electronic process in non-crystalline materials. Oxford University Press; 1979.
[42] Saravanan S, Anantharaman M, Venkatachela S. Composition and structure characterization of aluminum after laser ablation. Mater Sci Eng B 2006;135:108–12.
[43] Javed AK, Mohd Q, Braj RS, Sneha S, Mohd S, Wasi K, et al. Synthesis and characterization of structural, optical, thermal and dielectric properties of polyaniline/$CoFe_2O_4$ nanocomposites with special reference to photocatalytic activity. Spectrosc Acta A 2013;109:313–21.
[44] Rand BP, Forrest SR. Long range absorption enhancement in organic tandem thin film solar cells containing silver nanoclusters. J Appl Phys 2004;96:7519–26.
[45] Schaadt DM, Feng B, Yu ET. Enhanced semiconductor optical absorption via surface plasmon excitation in metal nanoparticles. Appl Phys Lett 2005;86, 063106-1–063106-3.
[46] Mostafa AJ, Rowlen KL, Reilly TH, Romero MJ, van de Legamaat J. Plasmon-enhanced solar energy conversion in organic bulk heterojunction photovoltaics. Appl Phys Lett 2008:92, 013504-1–013504-3.
[47] Jestl M, Maran I, Kock A, Beinsting W, Gornik E. Polarization-sensitive surface plasmon Schotky detectors. Opt Lett 1989;14:719–21.
[48] Manawwer A, Anees AA, Mohammed RS, Naser AM. Optical and electrical conducting properties of polyaniline/tin oxide nanocomposite. Arab J Chem 2013;6:341–5.
[49] Javed AK, Mohd Q, Braj RS, Sneha S, Mohd S, Wasi K, et al. Synthesis and characterization of structural, optical, thermal and dielectric properties of polyaniline/$CoFe_2O_4$ nanocomposites with special reference to photocatalytic activity. Spectrochim Acta A 2013;109:313–21.